Article

Cite This: *Biomacromolecules* XXXX, XXX, XXX−XXX

pubs.acs.org/Biomac

Glycocalyx-Mimicking Nanoparticles Improve Anti-PD-L1 Cancer Immunotherapy through Reversion of Tumor-Associated Macrophages

Yufei Zhang,[†] Libin Wu,[†] Zhen Li,[†] Weiyi Zhang,[†] Feifei Luo,[‡] Yiwei Chu,[§] and Guosong Chen*[,†]

[†]Department of Macromolecular Science, The State Key Laboratory of Molecular Engineering of Polymers, Fudan University, Shanghai, 200438, China

[‡]Department of Digestive Diseases, Huashan Hospital, Fudan University, Shanghai, 200040, China

[§]Department of Immunology, School of Basic Medical Sciences, Fudan University, Shanghai, 200032, China

Supporting Information

ABSTRACT: Immune checkpoint blockade by anti-PD-L1 monoclonal antibody (αPD-L1) has achieved unprecedented clinical benefits in certain cancers, whereas the therapeutic efficacy is often hindered by immunosuppressive tumor microenvironment mediated by tumor-associated macrophages (TAMs), which leads to innate resistance to this approach. To improve checkpoint blockade efficacy, the amphiphilic diblock copolymers poly(mannopyranoside/galactopyranoside methacrylate)-*block*-polystyrene are prepared by RAFT polymerization, which are sequentially self-assembled into glycocalyx-mimicking nanoparticles (GNPs) to neutralize TAMs. It is shown that GNPs can be specifically internalized by TAMs via lectin receptors, which results in upregulation of immunostimulatory IL-12 and downregulation of immunosuppressive IL-10, arginase 1, and CCL22, indicating functional reversion of protumor TAMs toward antitumor phenotype. The reversion of TAMs is proved to be mainly controlled by suppressing STAT6 and activating NF-κB phosphorylation. In vivo therapeutic studies have demonstrated that GNPs significantly enhance the therapeutic efficacy of αPD-L1 cancer therapy by reduction of tumor burden. Moreover, combination therapies with GNPs and αPD-L1 greatly improve immunosuppressive tumor microenvironment by reciprocal modulation of tumor-infiltrating effector and regulatory T cells. Notably, for the first time, our results demonstrate the reversion of TAMs and improvement of αPD-L1 cancer therapy by synthetic carbohydrate-containing nanomaterials. This research highlights a promising strategy for optimizing immune checkpoint blockade in cancer immunotherapy.

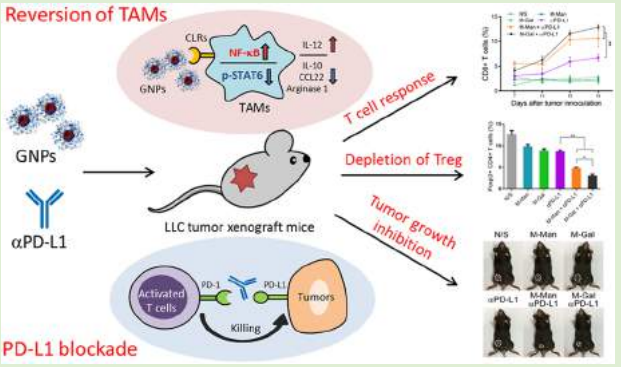

INTRODUCTION

Immune checkpoint blockade is a recent development in cancer immunotherapy which has shown impressive therapeutic benefits in certain cancers.[1−3] Immune checkpoints refer to a number of inhibitory proteins of the immune system to maintain homeostasis and self-tolerance.[4] Under normal physiological conditions, immune checkpoints are crucial for protection of autoimmunity and tissue damage from excessive activation of immune system,[5] whereas the expression of these inhibitory proteins can be widely dysregulated by tumors as an important immune evasion mechanism. Programmed death-ligand 1 (PD-L1) is one of the crucial immune checkpoint proteins highly associated with tumor escape from immune attack.[6] PD-L1 is rarely expressed on normal epithelial tissues but is abundantly expressed on many tumor cells including lung cancer, breast cancer, and melanoma.[7−9] The binding of PD-L1 with its receptor programmed death-1 (PD-1) exhaust T cells by suppressing the secretion of IFN-γ, perforin and granzyme, which ultimately leads to tumor progression and metastasis.[10]

Currently, the most effective checkpoint inhibitors are anti-PD-L1 monoclonal antibodies (αPD-L1), such as atezolizumab, which recently has been approved by FDA.[11,12] These mAbs function through blocking the PD-1/PD-L1 axis to reinvigorate exhausted tumor-specific T cells and restore antitumor immunity.[13] However, ongoing clinical trials have shown an innate resistance to PD-L1 blockade.[14] A majority of cancer patients do not have durable clinical benefits.[15] The mechanisms of PD-L1 resistance are complex. A couple of very recent and important studies have demonstrated that immunosuppressive tumor microenvironment induced by distinct protumor immune cells plays pivotal roles in maintaining this resistance.[16,17] These studies demonstrate

Special Issue: Biomacromolecules Asian Special Issue

Received: February 20, 2018
Revised: April 6, 2018
Published: April 10, 2018

DOI: 10.1021/acs.biomac.8b00305
Biomacromolecules XXXX, XXX, XXX−XXX

therapies targeting immunosuppressive cells combined with checkpoint blockade inhibitors to overcome the tumor resistance and reinstate effective antitumor immunity.[18,19]

Tumor-associated macrophages (TAMs) are the dominant type of the immunosuppressive cells during tumor progression.[20,21] Although macrophages have the potential to fight with tumor cells and trigger tumor-destructive responses, accumulating evidence have confirmed that TAMs are influenced by the signals originating from tumor cells to promote immunosuppression, angiogenesis, invasion, and metastasis.[22−24] TAMs in progressing neoplasms typically express characteristic surface C-type lectin receptors (CLRs), such as macrophage mannose receptor (MMR, CD206) and macrophage galactose-type lectin (MGL, CD301).[25] CD206 contains eight extracellular carbohydrate-recognition domains (CRDs) on a rigid scaffold, which recognizes terminal mannose, *N*-acetylglucosamine, and fucose residues of glycans.[26] CD301 has a different structure that contains a cluster of three CRDs supported by a coiled-coil peptide scaffold, which recognizes terminal galactose and *N*-acetylgalactosamine.[27] These lectin receptors in physiological conditions recognize carbohydrate moieties of the membrane glycolipids and glycoproteins on the surface of pathogens, also known as glycocalyx. Both of CD206 and CD301 contain intracellular domains to induce strong endocytosis effect and immune activation of macrophages.[28] In our previous work, we have demonstrated that glycocalyx-mimicking nanoparticles (GNPs) could efficiently polarize alternative-activated macrophage (M2) toward classical-activated phenotype (M1).[29] In consideration of M1, the macrophage has an immunostimulatory phenotype which distinguishes from the immunosuppressive M2 macrophage, and it is reasonable to hypothesize GNPs could also modulate M2-like TAMs by reduction of suppressive functions and eventually to facilitate cancer immunotherapy.

Therefore, aiming at improving immune checkpoint blockade in cancer therapy, especially αPD-L1 therapy, in this study we synthesized amphiphilic diblock copolymers modified with mannopyranoside or galactopyranoside. The diblock copolymers were employed to self-assemble into mannose/galactose-functionalized nanoparticles. The self-assembled GNPs enable the carbohydrates at a very high density on the surface, which significantly enhance the specific interaction with lectin receptors through the "cluster glycoside effect" compared to glycopolymers.[30] These GNPs were then used to modulate immunosuppressive TAMs by targeting CD206 and CD301, respectively. We found these GNPs were featured by specific binding activity with these lectin receptors. Engagement of GNPs was able to modulate TAMs by increasing immunostimulatory IL-12 secretion and reducing immunosuppressive IL-10, arginase 1, and CCL22, which reversed TAMs toward antitumor phenotype. The reversion of TAMs was mainly dependent on the downregulation of STAT6 phosphorylation and upregulation of NF-κB p65 phosphorylation. Moreover, in vivo therapeutic studies have demonstrated that GNPs were able to enhance the therapeutic effect of αPD-L1 cancer therapy by significant reduction of tumor burden. Furthermore, combination therapies with GNPs and αPD-L1 greatly improved immunosuppressive tumor microenvironment by reciprocal modulation of tumor-infiltrating effector and regulatory T cells. Our results demonstrated the ability of these GNPs on reversion of TAMs and improvement of αPD-L1 cancer therapy, highlighting their great potential in cancer immunotherapy.

EXPERIMENTAL SECTION

Synthesis and Characterizations. The amphiphilic diblock copolymers were synthesized by the combination of reversible addition−fragmentation chain transfer (RAFT) polymerization and postpolymerization modification following our previous procedure.[29] Synthesis of poly(mannopyranoside methacrylate)-*block*-polystyrene (**PMan-*b*-PS**) is demonstrated as an example in the Supporting Information. ^{1}H nuclear magnetic resonance (NMR) spectra were performed with a 400 MHz Bruker instrument by using $CDCl_3$, CD_3OD, or DMSO-d_6 as solvents, and the acquired data were analyzed with Mnova software. Gel permeation chromatography (GPC) analysis was carried out with a Waters Breeze 1515 GPC analysis system with TSK gel α-2500, 3000 columns, using DMF with 0.5 M LiBr as eluents at a flow rate of 1 mL/min at 80 °C, and a PEO calibration kit (TOSOH) as the calibration standard. Dynamic light scattering (DLS) and zeta potential studies were taken by Zeta Sizer Nano ZS90 from Malvern Instruments. Transmission electron microscopy (TEM) images were taken with Tecnai G^2 instrument operating at an accelerating voltage of 200 kV.

Cell Line and Animal Model. Lewis lung carcinoma (LLC) tumor cells syngeneic with C57BL/6 mice were cultured in complete RPMI 1640 culture medium (Gibco) supplemented with 10% fetal bovine serum (Gibco), 100 IU/mL of penicillin (Gibco), and 100 μg/mL of streptomycin (Gibco). Cells were maintained under fully humidified atmosphere at 37 °C and 5% CO_2 conditions. C57BL/6 mice were purchased from Shanghai SLAC Laboratory Animal Company. All animals were maintained in specific pathogen-free condition. Animal experiments were performed according to the Guidelines of Fudan University for the Care and Use of Laboratory Animals. LLC tumor xenograft mice were established by subcutaneous inoculation with 1×10^5 LLC tumor cells in the right inguen. LLC tumor xenograft mice were used for either TAMs isolation or therapeutic experiments.

Isolation of TAMs. Two weeks after the initial inoculation of LLC tumor cells, tumor tissues were mechanically excised and dissociated into small pieces followed by enzymatically digestion with collagenase IV (0.5 mg/mL, Sigma-Aldrich) and DNase I (50 IU/mL, Sigma-Aldrich) for 1 h. Red blood cells were removed by treating with ACK lysing buffer (Gibco). Tumor tissues were then filtrated through 70 μm cell strainers (Falcon) to obtain the single cell suspension. TAMs were isolated under magnetic-activated cell sorting (MACS) technology. Briefly, single cell suspension was first stained with anti-F4/80-biotin antibody (Miltenyi) for 10 min then magnetically stained with antibiotin MicroBeads (Miltenyi) for 15 min. Cells were resuspended with MACS separation buffer to go through LS columns (Miltenyi) in the magnetic field. The magnetically labeled F4/80+ cells were retained on the column after removal from the magnetic field and were collected as TAMs by flushing the column. To analyze the surface markers, TAMs were incubated with anti-CD16/CD32 antibody (BioLegend) to block nonspecific Fc-mediated interactions, and then stained with anti-F4/80, anti-CD11b, anti-CD206 and anti-CD301 fluorescent antibodies (BioLegend). The expression of these markers was detected under flow cytometry (Gallios, Beckman).

Cell Viability Assay. Cell viability assay was performed by using Cell Counting Kit-8 (CCK-8, Dojindo) to detect dehydrogenase activity under both time- and dose-dependent experiments. Briefly, TAMs were treated with different concentration of GNPs (from 1 μg/mL to 1 mg/mL) for a fixed incubation time of 72 h or containing 1 mg/mL of GNPs for a range of incubation time from 24 to 72 h. CCK-8 reagent was added into cell culture and incubated for 2 h. The absorbance was measured at 450 nm using a microplate reader (BioTek ELx800).

Cellular Uptake Experiment. Cellular uptake of fluorescent GNPs in vitro was performed under both time- and dose-dependent experiments. TAMs were treated with different amounts of fluorescent GNPs from 0.1 to 100 μg/mL for 4 h or with 10 μg/mL of fluorescent GNPs for a range of incubation time from 1 to 24 h. TAMs were harvested from culture plates by cell scrapers. The intracellular fluorescent intensity was measured by flow cytometry. To inhibit

DOI: 10.1021/acs.biomac.8b00305
Biomacromolecules XXXX, XXX, XXX−XXX

cellular uptake of fluorescent GNPs in vitro, TAMs were incubated with different concentrations of anti-CD206 or anti-CD301 blocking antibodies (from 3 to 100 μg/mL) for 2 h followed by addition of fluorescent GNPs (10 μg/mL) for 4 h. The intracellular fluorescent intensity was detected by flow cytometry. To analyze cellular uptake of fluorescent GNPs in vivo, LLC tumor xenograft mice were received subcutaneous injection of fluorescent GNPs (50 μg) adjacent to the tumors at day 7. Two days after injection, tumor tissues were mechanically excised and enzymatically digested. Single cell suspension was first incubated with anti-CD16/CD32 antibody followed by staining with anti-CD45, anti-F4/80, anti-CD11c, anti-Gr-1, anti-B220, anti-CD3, and anti-NK1.1 fluorescent antibodies (BioLegend). Intracellular fluorescent intensity of each cellular subset was detected under flow cytometry.

Confocal Imaging. To trace the intracellular uptake of fluorescent GNPs, TAMs were seeded on 35 mm glass bottom cell culture dishes (NEST) in complete culture medium containing 10 μg/mL of fluorescent GNPs for 4 h. Lysosomes were stained with 100 nM of deep-red LysoTracker (Life technologies) for extra 2 h. TAMs were then fixed with 4% paraformaldehyde. The nuclei were stained with 3 μM DAPI (BioLegend). Fluorescent images of TAMs were obtained using confocal microscopy (Nikon C2+) with an excitation wavelength at 488 nm for fluorescent GNPs, 561 nm for LysoTracker, and 405 nm for DAPI. Images were analyzed under NIS-Elements Viewer software (Nikon).

Gene Expression Analysis by Quantitative Real-Time PCR (qPCR). To analyze gene expression of cellular mediators, TAMs were incubated with GNPs (20 μg/mL) for 6 h with or without anti-CD206 or anti-CD301 blocking antibodies (10 μg/mL). Total RNA was extracted using MiniBEST Universal RNA Extraction Kit (Takara). cDNA was synthesized from total RNA using the primerScript RT reagent Kit (Takara). qPCR was performed in triplicate for each sample by the FastStart Universal SYBR Green Master Kit (Takara) and conducted on Applied Biosystems 7500 real-time PCR system. Data analysis was under ABI 7500 software. Primer oligonucleotides were designed by the Primer Premier software and synthesized by Shanghai Sangon Biotech. β-Actin was used as a housekeeping gene for normalization. All primer sequences were listed in Supporting Information, Table S1.

Cellular Mediator Detection. To analyze IL-12, IL-10, and CCL22 secretion, TAMs were incubated with GNPs (20 μg/mL) for 24 h with or without anti-CD206 or anti-CD301 blocking antibodies (10 μg/mL). Culture supernatant was collected and detected by enzyme-linked immunosorbent assay (ELISA) kits (R&D systems) following the manufacturer's procedures. The activity of arginase 1 was detected by an Arginase Assay Kit (Abnova). Briefly, TAMs were harvested and treated with 1 μM pepstatin A (Sigma-Aldrich), 1 μM leupeptin (Sigma-Aldrich), and 0.5% (w/v) Triton X-100 (Sigma-Aldrich). Supernatant was collected for arginase 1 detection. To detect cellular mediators secretion in vivo, LLC tumor xenograft mice subcutaneously received GNPs (50 μg) treatment adjacent to the tumor. Treatment was conducted every 4 days for a total of 5 times (days 2, 6, 10, 14, 18). One day after the last treatment, tumor tissues were mechanically excised and homogenized in PBS containing 0.5% (w/v) Triton X-100 with Dounce homogenizers. Tumor homogenate was centrifuged to collect supernatant for cellular mediator detection.

Phospho-Flow Cytometry. TAMs were treated with GNPs (20 μg/mL) for 30 min and then fixed in 4% paraformaldehyde for 10 min, immediately followed by permeabilization in ice-cold 100% methanol for 30 min. After suspension in staining buffer, TAMs were incubated with phospho-specific antibodies for 1 h prior to flow cytometry analysis. To inhibit NF-κB activation, TAMs were pretreated with 10 μM BAY 11-7082 (Sigma-Aldrich) for 1 h before GNPs stimulation. All phospho-specific antibodies and buffer were purchased from BDbiosciences. Data were analyzed under FlowJo software.

T Cell Activation and Proliferation Analysis. T cells were isolated from spleen of C57BL/6 mice by CD3ε MicroBead MACS isolation kit (Miltenyi) and stained with 2.5 μM carboxyfluorescein succinimidyl ester (CFSE, BioLegend) to obtain CFSE-T cells. TAMs were coincubated with CFSE-T cells at a ratio of 1/4 on U-bottom plates in the presence of anti-CD3 (5 μg/mL, precoated, BioLegend) and anti-CD28 (2 μg/mL, soluble, BioLegend) antibodies for T cell activation. Cell mixture was then treated with GNPs (20 μg/mL) for 72 h. As controls, cell mixture was additionally treated with anti-CD206 or anti-CD301 antibodies (10 μg/mL), respectively. T cell proliferation was measured by CFSE dilution gated on CD3+ cells by flow cytometry. To exclude the possibility that GNPs directly stimulate T cells, CFSE-T cells were treated with GNPs (20 μg/mL) in the presence of anti-CD3/28 for 72 h. The CFSE dilution was measured gated on CD3+ cells by flow cytometry. To analyze T cell activation, unlabeled T cells were coincubated with TAMs in the presence of anti-CD3/28. The cell mixture was treated with GNPs (20 μg/mL) for 12 h. Then cell mixture was stained with anti-CD3, anti-CD25, and anti-CD69 fluorescent antibodies for flow cytometry analysis.

In Vivo Therapeutic Experiments. LLC tumor xenograft mice received administration of αPD-L1 antibody (50 μg, BioLegend) intravenously and GNPs (50 μg) subcutaneously adjacent to the tumors at days 2, 6, 10, 14, 18. As controls, mice also received monotherapy with αPD-L1 or GNPs, respectively. Tumor growth was monitored every 4 days. The tumor area was measured with a digital caliper and calculated using the formula: largest diameter × smallest diameter. To analyze T cell infiltration in tumor tissues, 24 h after each injection (day 7, 11, 15, 19), tumor tissues were mechanically excised and enzymatically digested. Single cell suspension was first incubated with anti-CD16/CD32 to block nonspecific Fc-mediated interactions and then stained with anti-CD45, anti-CD4, and anti-CD8 fluorescent antibodies (BioLegend) to distinguish helper T cell and cytotoxic T cell. To analyze effector T cells and regulatory T cells, single cell suspension from the end point of treatment was intracellularly stained with anti-IFN-γ and anti-Foxp3 fluorescent antibodies (BioLegend). Experiments were performed under flow cytometry. All staining buffer and isotype antibodies were purchased from BioLegend. Data analysis was under FlowJo software.

Statistical Analysis. Results are shown as means ± SEM as indicated. Statistical significance was calculated by Student's *t*-test or One-way ANOVA. * $p < 0.05$, ** $p < 0.01$. Statistical analysis was performed under GraphPad Prism software.

RESULTS AND DISCUSSION

Synthesis, Self-Assembly, and Characterizations of GNPs. The diblock copolymers **PMan-*b*-PS** and **PGal-*b*-PS** were synthesized by two-step RAFT polymerization followed by postpolymerization modification via click chemistry with either mannopyranoside or galactopyranoside (Figure 1a and Scheme 1). The diblock copolymers contained a hydrophobic polystyrene (PS) block and a hydrophilic glyco-block. The results of the polymerization are shown in Table 1 and Supporting Information, Figure S1. ^{1}H NMR spectroscopic analysis confirmed the successful synthesis of the two diblock copolymers and their precursors (Supporting Information, Figure S1). The degree of polymerization (DP) of glyco-block was found to be 47 and the DP of PS block was found to be 158 according to the NMR spectra. GPC analysis was also employed to characterize the diblock copolymers supporting narrow polydispersity (PDI < 1.20) (Table 1). The amphiphilic polymers were self-assembled in aqueous solution into GNPs with a compact glyco-shell and an inert organic PS core. According to their different glyco-shells, the GNPs were marked as **M-Man** (mannose-functionalized nanoparticles) and **M-Gal** (galactose-functionalized nanoparticles), respectively (Figure 1a). DLS measurements showed that the diameters of **M-Man** and **M-Gal** were about 25 and 24 nm with a narrow distribution (PDI = 0.10) (Figure 1b and Table 2), respectively. TEM images confirmed their morphology as sphere nanoparticles (Figure 1c). Zeta potential measurements also confirmed the neutral surface property of **M-Man** and **M-Gal**

DOI: 10.1021/acs.biomac.8b00305
Biomacromolecules XXXX, XXX, XXX−XXX

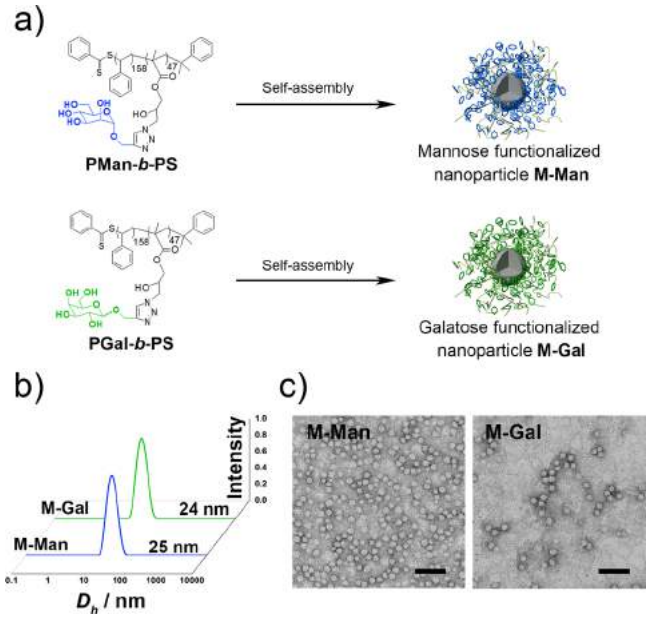

Figure 1. (a) Self-assembly of diblock copolymers **PMan-*b*-PS** and **PGal-*b*-PS** into **M-Man** and **M-Gal**, respectively. (b) DLS characterization of **M-Man** and **M-Gal** in PBS (pH 7.2, 10 mM). (c) TEM images of **M-Man** and **M-Gal** (scale bar 100 nm).

(−7.36 and −5.97 mV) in PBS (pH 7.2, 10 mM) (Table 2). Collectively, these characterizations confirmed the uniformity of these nanoparticles, which ensured the reproducibility of the subsequent immunological research.

Specific Internalization of GNPs by TAMs. TAMs were isolated from LLC tumor xenograft mice by MACS technology. Tumor was mechanically excised and single cell suspension was prepared by enzymatically digestion. F4/80 is a cell surface glycoprotein expressed in high levels on various macrophages including TAMs.[31] Thus, single cell suspension prepared from LLC solid tumors was magnetically labeled with anti-F4/80 antibody. Then F4/80-labeled cells that were positive were isolated from cell suspension as purified TAMs. Flow cytometry analysis confirmed that TAMs highly expressed F4/80 and myeloid marker CD11b (Figure 2a), which indicated the high purity of the isolated TAMs. Lectin receptors expressed by macrophages are dynamic, largely dependent on the milieus where the macrophages locate.[32] To determine whether TAMs express characteristic surface lectin receptors, we compared the expression of CD206 and CD301 between TAMs and murine peritoneal macrophages. It was found that TAMs expressed significantly higher levels of CD206 and CD301 compared to the peritoneal macrophages (Figure 2a), which provide specific receptors for GNPs recognition. Prior to performing the cellular uptake experiments, the cytotoxicity evaluation of GNPs were first performed by cell viability assays, as cell death caused by the toxicity of nanoparticles may result in disturbed cellular uptake behaviors. As shown in Supporting Information, Figure S2, both **M-Man** and **M-Gal** showed no obvious cytotoxicity toward TAMs below the concentration of 1 mg/mL for up to 72 h, which confirmed their good biocompatibility.

Table 1. M_n and PDI of Diblock Copolymers and Their Precursors

polymers[a]	M_n (^{1}H NMR)	M_n (GPC)	M_w/M_n[b] (GPC)
PG_{47}	6900	2700	1.13
PG_{47}-*b*-PS_{158}	23400	6300	1.11
PGA_{47}-*b*-PS_{158}	25100	7400	1.12
$Pman_{47}$-*b*-PS_{158}	35400	10800	1.16
$PGal_{47}$-*b*-PS_{158}	35400	11000	1.15

[a]Calculated from M_n obtained in ^{1}H NMR. [b]Measured by DMF GPC with PEG as calibration standard.

Table 2. Characterizations of M-Man and M-Gal

glycopolymers	GNPs	diameter [D_h]	PDI	zeta potential[a]
$PMan_{47}$-*b*-PS_{158}	**M-Man**	25	0.10	−7.36
$PGal_{47}$-*b*-PS_{158}	**M-Gal**	24	0.10	−5.97

[a]Measured in PBS (pH 7.2, 10 mM) at room temperature.

Scheme 1. Synthetic Route of Diblock Copolymer PMan-*b*-PS by Two-Step RAFT Polymerization and Postpolymerization Modification

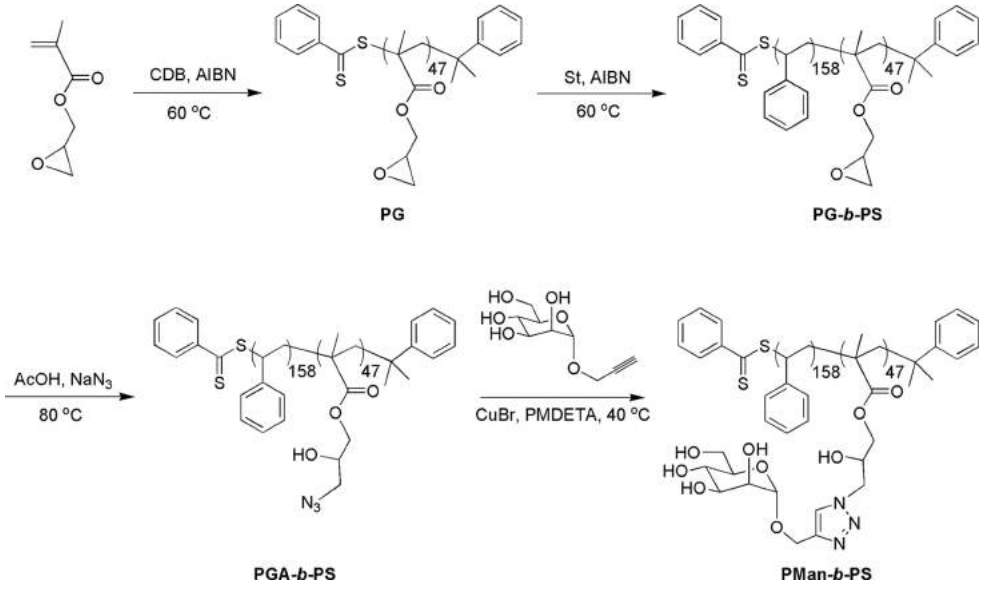

DOI: 10.1021/acs.biomac.8b00305
Biomacromolecules XXXX, XXX, XXX−XXX

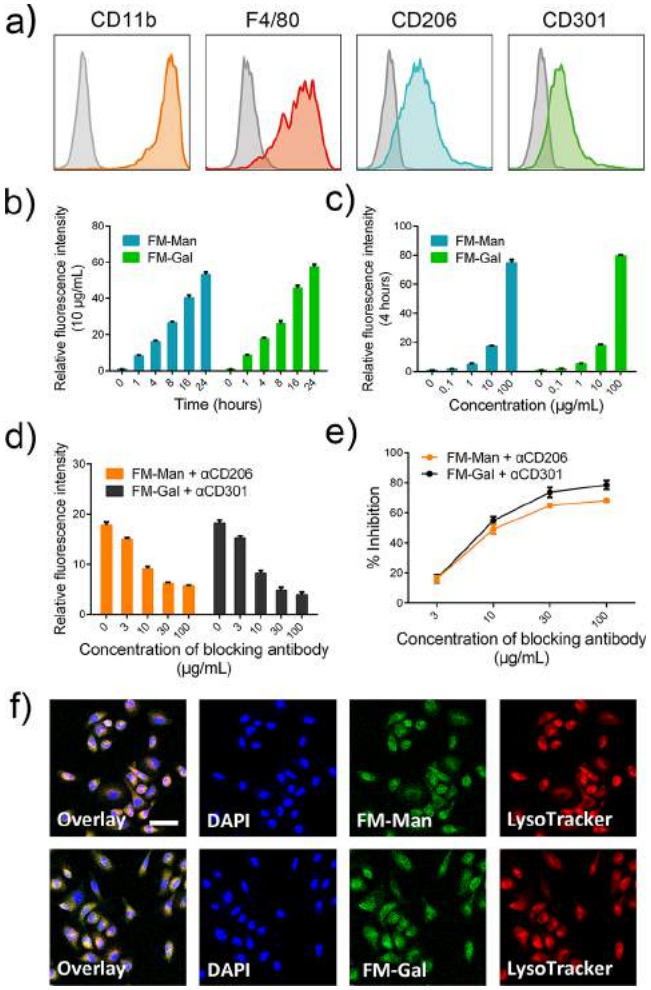

Figure 2. GNPs were internalized by TAMs via their specific lectin receptors. (a) The surface markers analysis of TAMs by flow cytometry. Colored lines, TAMs; gray lines, isotype control (CD11b and F4/80), murine peritoneal macrophages (CD206 and CD301). (b) Time-dependent and (c) dose-dependent endocytosis of fluorescent GNPs by TAMs. (d,e) Inhibition of fluorescent GNPs endocytosis by specific blocking antibodies of lectin receptors. (f) Confocal microscopy images of fluorescent GNPs internalization (scale bar 20 μm). Mean ± SEM.

Both of CD206 and CD301 have intracellular domain to induce effective endocytosis, thus the cellular uptake behaviors of GNPs by TAMs were evaluated. To trace GNPs, fluorescein isothiocyanate (FITC) was introduced to the end of the copolymers by clicking *N*-(5-fluoresceinyl) maleimide to the polymer chains after converting the benzodithioate group to a thiol group using ethylenediamine as an aminolysis agent (Scheme 2). Fluorescent GNPs (**FM-Man** and **FM-Gal**) were prepared from the FITC-labeled diblock copolymers accordingly. Their fluorescent intensities were then adjusted to the same level before their incubation with TAMs. The quantitative study of TAMs uptake to fluorescent GNPs was performed by flow cytometry. The intracellular fluorescent intensity was used to represent the amount of GNPs internalized by TAMs. It was found that there was a gradual accumulation of fluorescent intensity as the incubation time or concentration increased, indicating the time- and dose-dependent manner of cellular uptake (Figure 2b,c).

To confirm the specificity of GNPs endocytosis, cellular uptake was blocked by lectin-specific blocking antibodies: anti-CD206 antibody (αCD206) and anti-CD301 antibody (αCD301). As shown in Figure 2d, the endocytosis of both **FM-Man** and **FM-Gal** were decreased after addition of blocking antibodies, and the inhibition efficiency was gradually enhanced as the concentration of blocking antibodies was increased. When 30 μg/mL blocking antibodies were used, the inhibition of **FM-Man** and **FM-Gal** were 62% and 74%, respectively (Figure 2e). These blocking experiments indicated a specific lectin receptor-mediated endocytosis of GNPs. Confocal microscopy was used to investigate the cellular uptake process of GNPs. After fluorescent GNPs were incubated with TAMs, deep-red LysoTracker was then added to label lysosomes. As shown in Figure 2f, the internalization of **FM-Man** and **FM-Gal** (shown in green) by TAMs were clearly observed. The internalized GNPs were also found to properly colocalize with lysosomes in confocal images. Collectively, these experiments suggested GNPs can be internalized by TAMs through the specific lectin receptor-mediated endocytosis.

TAMs Reversion by GNPs Stimulation. TAMs are drivers of tumor progression, secreting various immunosuppressive cellular mediators to harm antitumor immunity.[33] Thus, solid evidence of TAMs reversion came from different expression of these mediators. IL-12 is a pro-inflammatory cytokine to principally activate natural killer (NK) cells and induce the differentiation of T helper 1 (Th1) effectors, which contribute to antitumor immunity,[34,35] whereas IL-10 is antagonistically opposed to limit the extent of antitumor immunity by diminishing antigen presentation and inactivating Th1 cells.[36] TAMs are also found to secrete arginase 1 (Arg1) to anergize T cell by consuming L-arginine[37] and CCL22 to recruit inhibitory

Scheme 2. Synthetic Route of FITC-Labeled FITC-PG-*b*-PS via Thiol−ene Reaction

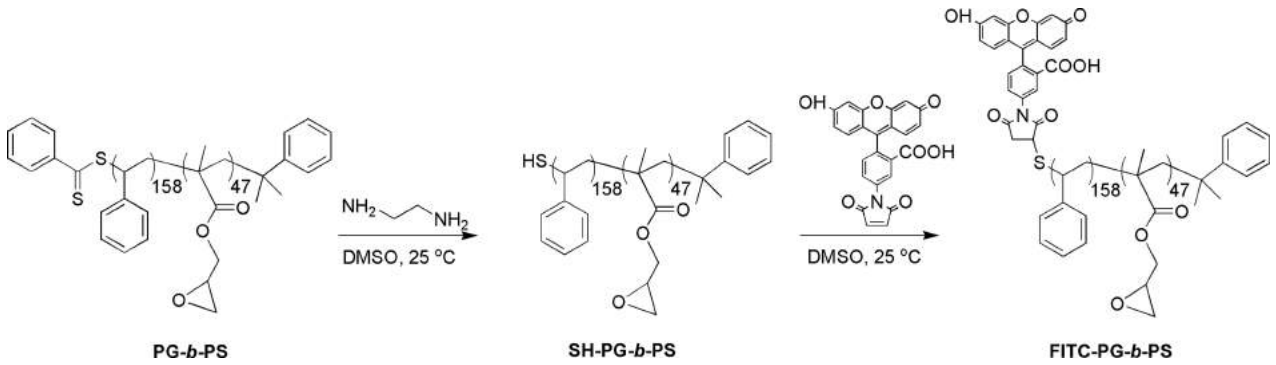

DOI: 10.1021/acs.biomac.8b00305
Biomacromolecules XXXX, XXX, XXX−XXX

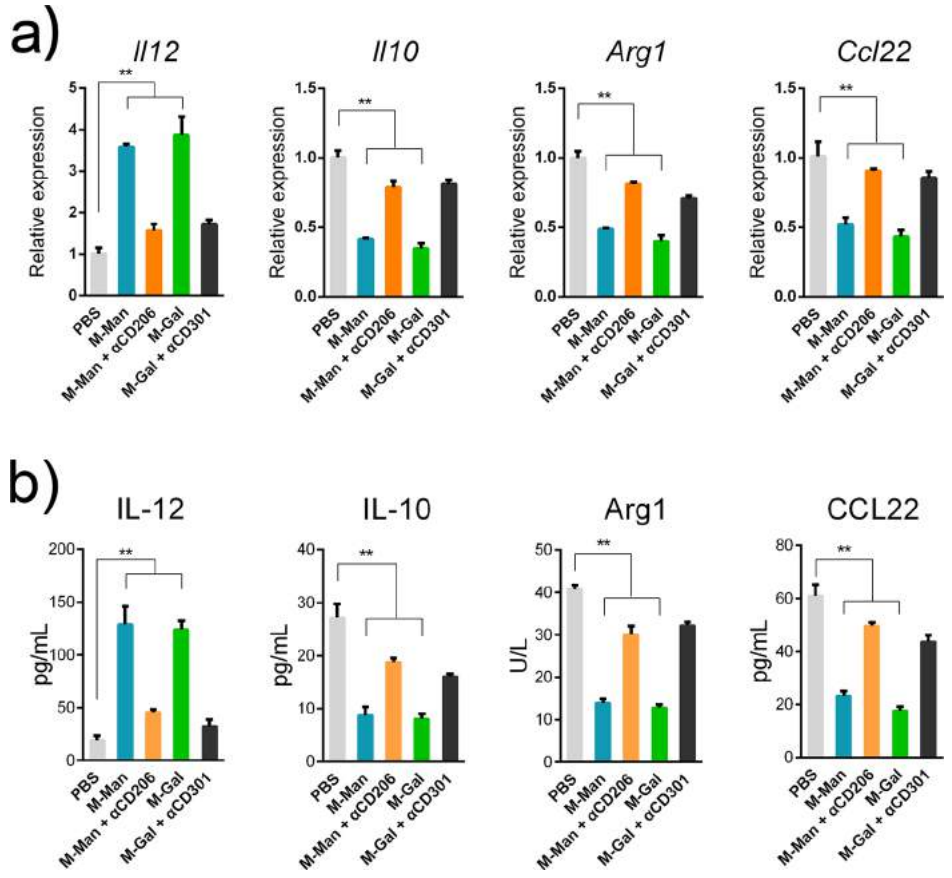

Figure 3. Immunosuppressive TAMs were functionally reversed by GNPs stimulation. (a) TAMs were treated with GNPs (20 μg/mL) for 6 h. Gene expression of *Ill2*, *Il10*, *Arg1*, and *Ccl22* by TAMs were detected by qPCR analysis. (b) TAMs were treated with GNPs (20 μg/mL) for 24 h. Protein release of IL-12, IL-10, Arg1, and CCL22 in supernatant by TAMs were detected by ELISA. Mean ± SEM. Student's *t*-test. * $p < 0.05$, ** $p < 0.01$.

regulatory T cells to further strengthen immunosuppression.[38,39] We further intended to investigate whether GNPs were able to modulate the expression of these key cellular mediators. Hence, TAMs were first incubated with **M-Man** or **M-Gal** (20 μg/mL) for 6 h. The gene expressions of these cellular mediators were analyzed by qPCR. As shown in Figure 3a, both of the GNPs stimulation significantly upregulated gene expression of *Il12*, whereas immunosuppressive genes expression of *Il10*, *Arg1*, and *Ccl22* were downregulated. The release of these mediators was also analyzed by ELISA. After TAMs were stimulated with GNPs (20 μg/mL) for 24 h, the supernatant was collected for protein quantification. The results were similar to the gene expression analysis. Pro-inflammatory IL-12 was promoted by GNPs stimulation and immunosuppressive IL-10, Arg1, and CCL22 were inhibited (Figure 3b). These results indicated that the immunosuppressive TAMs were functionally reversed by GNPs stimulation. Notably, the modulation of these cellular mediators were partially inhibited by CD206 or CD301 blocking antibodies (10 μg/mL), respectively, indicating that TAMs reversion was mediated through lectin receptor pathways.

Signaling Pathways Involved in TAMs Reversion. To investigate the signaling pathways involved in TAMs reversion, phosphorylated transcription factors related to macrophage activation and polarization were detected by phospho-flow cytometry. As shown in Figure 4a, tumor immunosuppression related phosphorylated STAT6 (p-STAT6) was significantly downregulated after GNPs stimulation. Meanwhile, p-NF-κB p65, the common downstream of lectin receptors, was significantly upregulated. However, p-STAT1, p-STAT3, p-ERK, p-Akt, and p-p38, which were reported to regulate macrophage activation and polarziation,[40−43] were not affected by GNPs stimulation. STAT6 is one of the vital transcription factors to maintain immunosuppression of TAMs. Activation of STAT6 is linked to the transcription of several immunosuppressive genes.[44] Because STAT6 is reported to inhibit NF-κB pathway leading to immunosuppression,[40,45] we intended to investigate whether there was crosstalk between NF-κB and STAT6 in TAMs reversion. NF-κB inhibitor BAY 11-7082 was used to treat TAMs prior to GNPs stimulation. As shown in Figure 4b, the activation of NF-κB p65 was totally inhibited, whereas p-STAT6 was still downregulated by GNPs stimulation. These results indicated that GNPs can induce the downregulation of p-STAT6 independent to the upregulation of p-NF-κB p65.

To further determine whether regulation of STAT6 and NF-κB phosphorylation is essential to TAMs reversion, a high amount of IL-4 (100 ng/mL) was used to maintain persistent activation of STAT6 in TAMs.[46] The downregulation of immunosuppressive IL-10, Arg1, and CCL22 by GNPs stimulation was totally inhibited (Figure 4c). In contrast, NF-κB inhibitor BAY 11-7082 could hardly influence the expression of these mediators (Figure 4d), indicating these immunosuppressive cellular mediators were mainly controlled by STAT6. Surprisingly, the upregulated IL-12 by GNPs stimulation was blocked by both IL-4 and BAY 11-7082 (Figure 4c,d), suggesting STAT6 and NF-κB function together to modulate the expression of IL-12. These results indicated that GNPs

DOI: 10.1021/acs.biomac.8b00305
Biomacromolecules XXXX, XXX, XXX−XXX

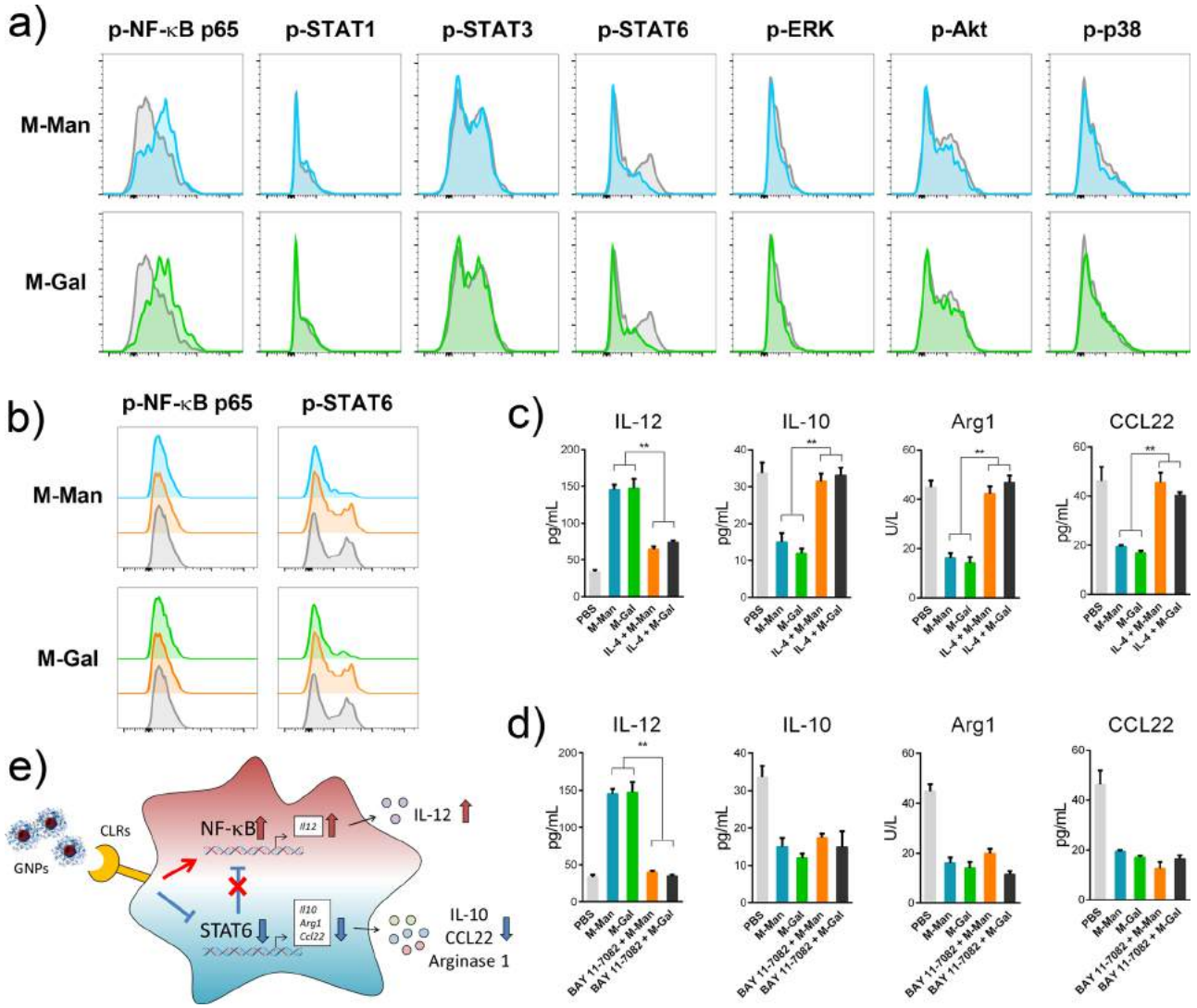

Figure 4. Reversion of TAMs was dependent on the reciprocal regulation of STAT6 and NF-κB signaling pathways. (a) Phosphorylated transcription factors related to TAMs activation and polarization were analyzed by phospho-flow cytometry after GNPs treatment (20 μg/mL) for 30 min (blue, **M-Man**; green, **M-Gal**). (b) p-NK-κB p65 and p-STAT6 were analyzed in TAMs treated with 10 μM NF-κB inhibitor BAY 11-7082 prior to GNPs stimulation by phospho-flow cytometry. (c) TAMs were treated with 100 ng/mL of IL-4 following GNPs stimulation for 24 h. (d) TAMs were treated with 10 μM of BAY 11-7082 following GNPs stimulation for 24 h. Secretion of IL-12, IL-10, Arg1, and CCL22 were determined by ELISA. (e) Schematic illustration of STAT6 and NF-κB signaling pathways by GNPs stimulation. Mean ± SEM. Student's *t*-test. * $p < 0.05$, ** $p < 0.01$.

stimulation led to reciprocal regulation of STAT6 and NF-κB signaling pathways, resulting in the functional reversion of TAMs (Figure 4e).

TAMs Reversion Contributed to T Cells Activation and Proliferation. T cells are well-known to play prominent roles in antitumor immunity, whereas the activity of T cells is greatly inhibited by immunosuppressive TAMs. To investigate whether T cells activation and proliferation would benefit from the reversion of TAMs, CFSE-labeled T (CFSE-T) cells were coincubated with TAMs followed by GNPs stimulation for 72 h. CFSE is a fluorescent dye that can be well-stained intracellularly and equally diluted as cell proliferation.[47] Cell mixture was cultured under anti-CD3/CD28 antibodies (αCD3/28) activation. As shown in Figure 5a, TAMs exhibited strong suppressive activity toward CFSE-T cells by inhibiting proliferation in PBS control. However, **M-Man** and **M-Gal** stimulation significantly promoted CFSE-T cells proliferation at ratios of 67.2% and 78.0%, respectively. Also, the enhanced proliferation could be inhibited by CD206 or CD301 blocking antibodies, which further highlighted the important role of lectin receptor pathways. In consideration of GNPs might directly promote CFSE-T cell proliferation, an additional assay without TAMs was performed to exclude this possibility. CFSE-T cell were directly treated with GNPs. CFSE dilution showed an average gradient among each group (Supporting Information, Figure S3), suggesting that enhanced T cell proliferation was dependent on the TAMs reversion but not individual GNPs stimulation toward T cells.

T cell activation is highly associated with remarkable expression of CD25 and CD69 molecules.[48] CD25, the α chain of IL-2 receptor plays an important role in mediating T cell proliferation, and CD69 is the earliest inducible cell surface glycoprotein during T cell activation. To evaluate T cell activation, TAMs and T cells were coincubated in the presence of GNPs stimulation for 12 h followed by flow cytometry analysis. We observed that GNPs led to a prominent increase of

DOI: 10.1021/acs.biomac.8b00305
Biomacromolecules XXXX, XXX, XXX−XXX

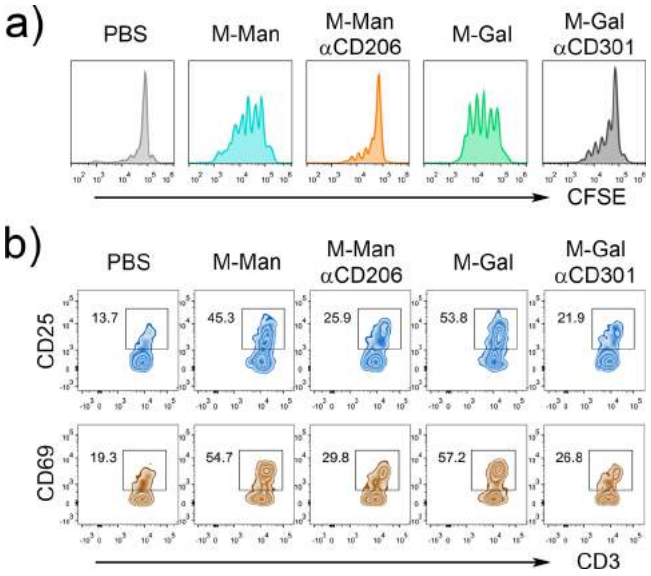

Figure 5. TAMs reversion contributed to T cells activation and proliferation. (a) CFSE-T cells were coincubated with TAMs under an effector/target (TAMs/T cells) ratio of 1/4 followed by GNPs stimulation (20 μg/mL) for 72 h. CFSE dilution was determined to monitor the generations of proliferating T cells by flow cytometry. (b) T cells were coincubated with TAMs followed by GNPs stimulation for 12 h. CD25 and CD69 expressed on T cells were analyzed by flow cytometry.

both molecules (Figure 5b), indicating strong activation of T cells. **M-Man** stimulated the increased expression of CD25 and CD69 at 45.3% and 54.7%, respectively, meanwhile **M-Gal** induced higher levels at 53.8% and 57.2%. Correspondingly, the activation markers were also downregulated by CD206 or CD301 blocking antibodies, which emphasized the interaction between GNPs and lectin receptors. Collectively, these results suggested that GNPs-induced TAMs reversion exhibited immunocompetent activity to promote T cells activation and proliferation.

Distribution of GNPs and Reversion of TAMs in Vivo. The ideal antitumor agents should exhibit antitumor properties both in vitro and in vivo. Encouraged by the notable ability of GNPs to modulate TAMs in vitro, we next investigated the distribution of GNPs and reversion of TAMs in LLC tumor xenograft mice in vivo. LLC tumor xenograft mice received single injection of fluorescent GNPs (50 μg) subcutaneously adjacent to the tumors at day 7. Tumor was mechanically excised and single cell suspension was prepared by enzymatically digestion. Cellular uptake of fluorescent GNPs was analyzed by the fluorescent intensity in each cellular subsets by flow cytometry. Tumor-infiltrating immune cells and LLC tumor cells were distinguished by staining with different fluorescent antibodies: TAMs (F4/80+), dendritic cells (CD11c+), granulocytes (Gr-1+), T cells (CD3+), B cells (B220+), NK cells (NK1.1+), and LLC tumor cells (CD45−). As shown in Figure 6a, fluorescent GNPs were mostly internalized by TAMs. The fluorescent intensity of TAMs was almost 3-fold higher than which of dendritic cells and more than 12-fold compared to control (Figure 6b), suggesting the efficient targeted ability of GNPs toward TAMs in vivo. To evaluate the reversion of TAMs in vivo, LLC tumor xenograft mice were treated with GNPs (50 μg) subcutaneously adjacent to the tumors every 4 days for 5 times before end-point analysis (Figure 7a). The intratumoral concentrations of cellular mediators were detected in the homogenized tumor tissues. Compared to the normal saline (N/S) group, GNPs treatment significantly upregulated the intratumoral secretion of pro-inflammatory IL-12 and meanwhile downregulated IL-10, Arg1,

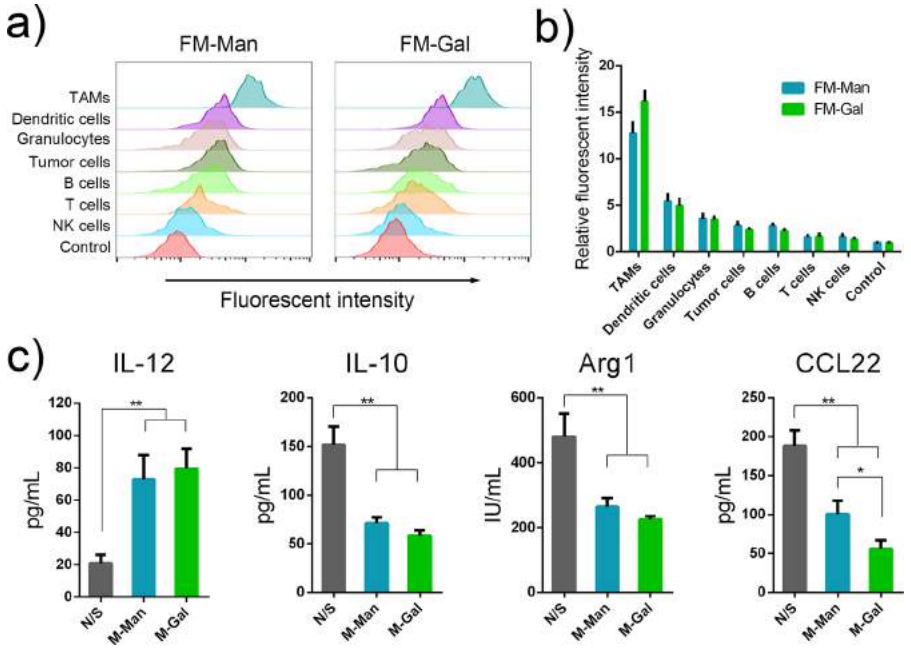

Figure 6. Distribution of GNPs and reversion of TAMs in vivo. (a) LLC tumor xenograft mice received single injection of fluorescent GNPs (50 μg) subcutaneously adjacent to the tumors at day 7. Intratumoral distribution in various cellular subsets was determined by flow cytometry. (b) Statistics of fluorescent intensity in each cellular subset. (c) LLC tumor xenograft mice received GNPs treatments (50 μg) subcutaneously adjacent to the tumors every 4 days for 5 times before end point analysis. IL-12, IL-10, Arg1, and CCL22 were determined in homogenized tumor tissues by ELISA. Mean ± SEM. Student's *t*-test. * $p < 0.05$, ** $p < 0.01$.

DOI: 10.1021/acs.biomac.8b00305
Biomacromolecules XXXX, XXX, XXX−XXX

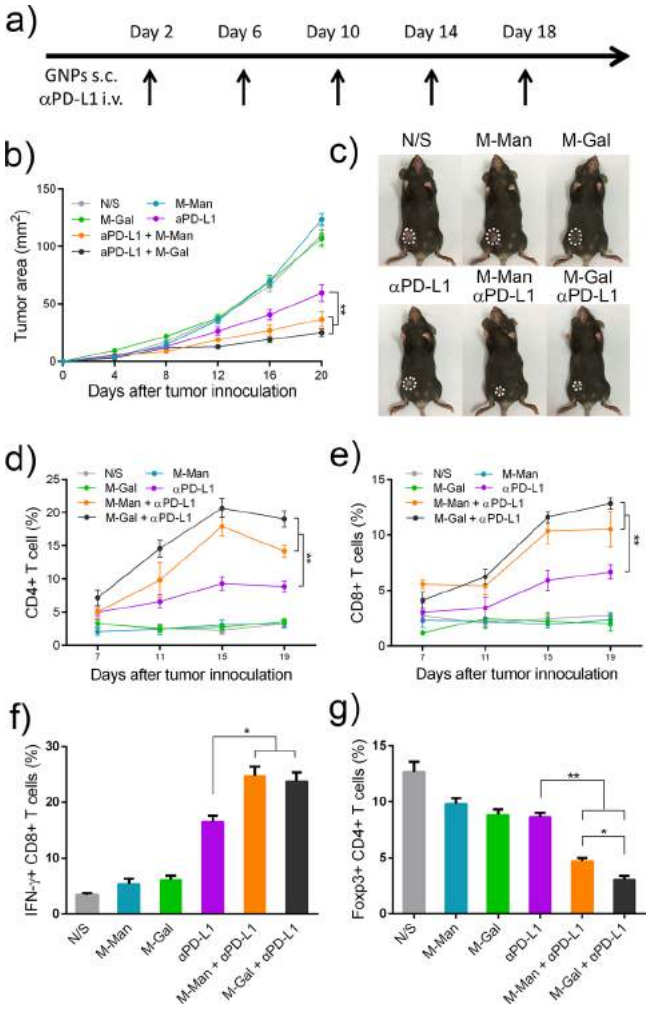

Figure 7. GNPs improved αPD-L1 blockade in cancer immunotherapy. (a) LLC tumor xenograft mice received combination therapies with αPD-L1 (50 μg) and GNPs (50 μg), or monotherapies with αPD-L1 or GNPs. (b) Tumor progression was monitored by measuring tumor volume. Five mice for each group (n = 5). (c) Representative mice of each group. (d,e) Infiltration of helper T cells (CD4+) and cytotoxic T cells (CD8+) in tumor were analyzed by flow cytometry. (f,g) Infiltration of effector T cells (IFN-γ+ CD8+) and regulatory T cells (Foxp3+ CD4+) in tumor were analyzed by flow cytometry. Mean ± SEM. Student's t-test (b,d,e). One-way ANOVA (f,g). * $p < 0.05$, ** $p < 0.01$.

and CCL22 (Figure 6c). Notably, we also noticed that **M-Gal** induced more reduction of CCL22 than **M-Man**. Collectively, these results demonstrated that GNPs were able to selectively target and reverse immunosuppressive TAMs by modulating the expression of cellular mediators in the tumor microenvironment.

GNPs Improved αPD-L1 Blockade in Cancer Immunotherapy. To explore whether GNPs were able to enhance immune checkpoint blockade in cancer immunotherapy, combination therapies with αPD-L1 and GNPs were performed to evaluate therapeutic efficacy. LLC tumor xenograft mice were randomized to receive combination therapies with injection of GNPs (50 μg) subcutaneously adjacent to the tumors and injection of αPD-L1 (50 μg) intravenously every 4 days for 5 times (Figure 7a). As controls, the mice were also received monotherapy with either GNPs or αPD-L1. Tumor diameters were measured 2 days after each injection to monitor tumor progression. As show in Figure 7b, GNPs monotherapies had minimal impact on LLC tumor remission compared to N/S control. Immune checkpoint blockade by αPD-L1 partially inhibited tumor growth. However, the results from the combination therapies were inspiring. Continued injections with αPD-L1 and GNPs significantly reduced tumor burdens compared to all monotherapies, suggesting that GNPs-induced TAMs reversion contributed to improvement of αPD-L1 therapy. The representative mice with white lines of tumor burden in each treatment group were shown in Figure 7c. Interestingly, **M-Gal** exhibited stronger ability on facilitating αPD-L1 blockade. Compared to N/S group, injections of αPD-L1 with **M-Man** or **M-Gal** inhibited ∼67% or ∼77% of the tumor growth, respectively.

Because combination therapies exhibited excellent efficacy on LLC tumor regression, T cells infiltration in tumors were further explored. Flow cytometry analysis was performed 24 h after each injection. It was found that combination therapies were associated with significant increase of both helper T cells (CD4+) and cytotoxic T cells (CD8+) infiltration compared to αPD-L1 monotherapy (Figure 7d,e). In addition, we observed more T cell infiltration induced by **M-Gal**. The enhanced T cell infiltration reached optimum at the end point of treatment, suggesting the persistent T cell response was induced during treatment. In contrast, GNPs monotherapy appeared to have no effect on T cell infiltration. Furthermore, the combination therapies showed optimal therapeutic property by reciprocal upregulation of effector T cells (IFN-γ+ CD8+) and downregulation of regulatory T cells (Foxp3+ CD4+) (Figure 7f,g). Notably, αPD-L1 therapy coupled with **M-Gal** induced less regulatory T cells infiltration than **M-Man**. It was mainly contributed by the much lower level of CCL22 induced by **M-Gal** in vivo. Taken together, our results demonstrated that GNPs not only induced functional reversion of TAMs, but also reciprocally regulated T cell response in tumor microenvironment, providing the optimal immune situation to improve αPD-L1 blockade in cancer immunotherapy.

CONCLUSIONS

In summary, diblock copolymers functionalized with either mannopyranoside or galactopyranoside were synthesized by RAFT polymerization and postpolymerization modification. We have demonstrated that glycocalyx-mimicking GNPs self-assembled from these copolymers had potent ability to reverse immunosuppressive TAMs both in vitro and in vivo. STAT6 and NF-κB signaling pathways were proved to control the TAMs reversion by GNPs. Furthermore, the TAMs reversion significantly improved tumor microenvironment by reciprocally regulating effector T cells and regulatory T cells, leading to improved therapeutic efficacy of αPD-L1 checkpoint blockade in cancer therapy. As we know, this is the first research to utilize synthetic carbohydrate-containing nanomaterials to enhance the antitumor effect of immune checkpoint blockade. Distinguished from natural polysaccharides from glycocalyx, self-assembled GNPs show better structural adjustability and offer the possibility of attaching different types of carbohydrates onto the same scaffold in a controlable way. This study highlights a novel and promising therapeutic strategy that overcoming resistance to immune checkpoint blockade, therefore providing a valuable avenue for optimizing cancer immunotherapy.

DOI: 10.1021/acs.biomac.8b00305
Biomacromolecules XXXX, XXX, XXX−XXX

■ ASSOCIATED CONTENT

Supporting Information

The Supporting Information is available free of charge on the ACS Publications website at DOI: 10.1021/acs.biomac.8b00305.

Synthesis of diblock copolymers and their precursors, self-assembly of GNPs, and primer sequences for qPCR analysis (PDF)

■ AUTHOR INFORMATION

Corresponding Author

*E-mail: guosong@fudan.edu.cn.

ORCID

Guosong Chen: 0000-0001-7089-911X

Notes

The authors declare no competing financial interest.

■ ACKNOWLEDGMENTS

We acknowledge the financial support from the National Natural Science Foundation of China (grant nos. 21504016 and 91527305).

■ REFERENCES

(1) Pardoll, D. M. The blockade of immune checkpoints in cancer immunotherapy. *Nat. Rev. Cancer* **2012**, *12*, 252−264.

(2) Topalian, S. L.; Drake, C. G.; Pardoll, D. M. Immune checkpoint blockade: a common denominator approach to cancer therapy. *Cancer Cell* **2015**, *27*, 450−461.

(3) Topalian, S. L.; Taube, J. M.; Anders, R. A.; Pardoll, D. M. Mechanism-driven biomarkers to guide immune checkpoint blockade in cancer therapy. *Nat. Rev. Cancer* **2016**, *16*, 275−287.

(4) Goodnow, C. C.; Sprent, J.; de St Groth, B. F.; Vinuesa, C. G. Cellular and genetic mechanisms of self tolerance and autoimmunity. *Nature* **2005**, *435*, 590−597.

(5) van der Vlist, M.; Kuball, J.; Radstake, T. R. D.; Meyaard, L. Immune checkpoints and rheumatic diseases: what can cancer immunotherapy teach us? *Nat. Rev. Rheumatol.* **2016**, *12*, 593−604.

(6) Dong, H.; Strome, S. E.; Salomao, D. R.; Tamura, H.; Hirano, F.; Flies, D. B.; Roche, P. C.; Lu, J.; Zhu, G.; Tamada, K.; Lennon, V. A.; Celis, E.; Chen, L. Tumor-associated B7-H1 promotes T-cell apoptosis: a potential mechanism of immune evasion. *Nat. Med.* **2002**, *8*, 793−800.

(7) Scheel, A. H.; Ansen, S.; Schultheis, A. M.; Scheffler, M.; Fischer, R. N.; Michels, S.; Hellmich, M.; George, J.; Zander, T.; Brockmann, M.; Stoelben, E.; Groen, H.; Timens, W.; Perner, S.; von Bergwelt-Baildon, M.; Buttner, R.; Wolf, J. PD-L1 expression in non-small cell lung cancer: Correlations with genetic alterations. *Oncoimmunology* **2016**, *5*, e1131379.

(8) Ghebeh, H.; Mohammed, S.; Al-Omair, A.; Qattan, A.; Lehe, C.; Al-Qudaihi, G.; Elkum, N.; Alshabanah, M.; Bin Amer, S.; Tulbah, A.; Ajarim, D.; Al-Tweigeri, T.; Dermime, S. The B7-H1 (PD-L1) T lymphocyte-inhibitory molecule is expressed in breast cancer patients with infiltrating ductal carcinoma: correlation with important high-risk prognostic factors. *Neoplasia* **2006**, *8*, 190−198.

(9) Hino, R.; Kabashima, K.; Kato, Y.; Yagi, H.; Nakamura, M.; Honjo, T.; Okazaki, T.; Tokura, Y. Tumor cell expression of programmed cell death-1 ligand 1 is a prognostic factor for malignant melanoma. *Cancer* **2010**, *116*, 1757−1766.

(10) Butte, M. J.; Keir, M. E.; Phamduy, T. B.; Sharpe, A. H.; Freeman, G. J. Programmed death-1 ligand 1 interacts specifically with the B7−1 costimulatory molecule to inhibit T cell responses. *Immunity* **2007**, *27*, 111−122.

(11) Rittmeyer, A.; Barlesi, F.; Waterkamp, D.; Park, K.; Ciardiello, F.; von Pawel, J.; Gadgeel, S. M.; Hida, T.; Kowalski, D. M.; Dols, M. C.; Cortinovis, D. L.; Leach, J.; Polikoff, J.; Barrios, C.; Kabbinavar, F.; Frontera, O. A.; De Marinis, F.; Turna, H.; Lee, J. S.; Ballinger, M.; Kowanetz, M.; He, P.; Chen, D. S.; Sandler, A.; Gandara, D. R. OAK Study Group. Atezolizumab versus docetaxel in patients with previously treated non-small-cell lung cancer (OAK): a phase 3, open-label, multicentre randomised controlled trial. *Lancet* **2017**, *389*, 255−265.

(12) Rosenberg, J. E.; Hoffman-Censits, J.; Powles, T.; van der Heijden, M. S.; Balar, A. V.; Necchi, A.; Dawson, N.; O'Donnell, P. H.; Balmanoukian, A.; Loriot, Y.; Srinivas, S.; Retz, M. M.; Grivas, P.; Joseph, R. W.; Galsky, M. D.; Fleming, M. T.; Petrylak, D. P.; Perez-Gracia, J. L.; Burris, H. A.; Castellano, D.; Canil, C.; Bellmunt, J.; Bajorin, D.; Nickles, D.; Bourgon, R.; Frampton, G. M.; Cui, N.; Mariathasan, S.; Abidoye, O.; Fine, G. D.; Dreicer, R. Atezolizumab in patients with locally advanced and metastatic urothelial carcinoma who have progressed following treatment with platinum-based chemotherapy: a single-arm, multicentre, phase 2 trial. *Lancet* **2016**, *387*, 1909−1920.

(13) Tumeh, P. C.; Harview, C. L.; Yearley, J. H.; Shintaku, I. P.; Taylor, E. J. M.; Robert, L.; Chmielowski, B.; Spasic, M.; Henry, G.; Ciobanu, V.; West, A. N.; Carmona, M.; Kivork, C.; Seja, E.; Cherry, G.; Gutierrez, A. J.; Grogan, T. R.; Mateus, C.; Tomasic, G.; Glaspy, J. A.; Emerson, R. O.; Robins, H.; Pierce, R. H.; Elashoff, D. A.; Robert, C.; Ribas, A. PD-1 blockade induces responses by inhibiting adaptive immune resistance. *Nature* **2014**, *515*, 568−571.

(14) O'Donnell, J. S.; Long, G. V.; Scolyer, R. A.; Teng, M. W.; Smyth, M. J. Resistance to PD1/PDL1 checkpoint inhibition. *Cancer Treat. Rev.* **2017**, *52*, 71−81.

(15) Heinzerling, L.; Kirchberger, M. C.; Walter, L.; Schuler, G. Predicting the response to anti-PD1 therapy in metastatic melanoma. *Transl. Cancer Res.* **2016**, *5*, S576−S579.

(16) Hugo, W.; Zaretsky, J. M.; Sun, L.; Song, C.; Moreno, B. H.; Hu-Lieskovan, S.; Berent-Maoz, B.; Pang, J.; Chmielowski, B.; Cherry, G.; Seja, E.; Lomeli, S.; Kong, X.; Kelley, M. C.; Sosman, J. A.; Johnson, D. B.; Ribas, A.; Lo, R. S. Genomic and Transcriptomic Features of Response to Anti-PD-1 Therapy in Metastatic Melanoma. *Cell* **2016**, *165*, 35−44.

(17) Lu, X.; Horner, J. W.; Paul, E.; Shang, X.; Troncoso, P.; Deng, P.; Jiang, S.; Chang, Q.; Spring, D. J.; Sharma, P.; Zebala, J. A.; Maeda, D. Y.; Wang, Y. A.; DePinho, R. A. Effective combinatorial immunotherapy for castration-resistant prostate cancer. *Nature* **2017**, *543*, 728−732.

(18) Bu, X.; Mahoney, K. M.; Freeman, G. J. Learning from PD-1 Resistance: New Combination Strategies. *Trends Mol. Med.* **2016**, *22*, 448−451.

(19) Mahoney, K. M.; Rennert, P. D.; Freeman, G. J. Combination cancer immunotherapy and new immunomodulatory targets. *Nat. Rev. Drug Discovery* **2015**, *14*, 561−584.

(20) Gajewski, T. F.; Schreiber, H.; Fu, Y.-X. Innate and adaptive immune cells in the tumor microenvironment. *Nat. Immunol.* **2013**, *14*, 1014−1022.

(21) Ostuni, R.; Kratochvill, F.; Murray, P. J.; Natoli, G. Macrophages and cancer: from mechanisms to therapeutic implications. *Trends Immunol.* **2015**, *36*, 229−239.

(22) Mantovani, A.; Allavena, P. The interaction of anticancer therapies with tumor-associated macrophages. *J. Exp. Med.* **2015**, *212*, 435−445.

(23) Noy, R.; Pollard, J. W. Tumor-associated macrophages: from mechanisms to therapy. *Immunity* **2014**, *41*, 49−61.

(24) Franklin, R. A.; Liao, W.; Sarkar, A.; Kim, M. V.; Bivona, M. R.; Liu, K.; Pamer, E. G.; Li, M. O. The cellular and molecular origin of tumor-associated macrophages. *Science* **2014**, *344*, 921−925.

(25) Yan, H.; Kamiya, T.; Suabjakyong, P.; Tsuji, N. M. Targeting C-Type Lectin Receptors for Cancer Immunity. *Front. Immunol.* **2015**, *6*, 408.

(26) Taylor, P. R.; Gordon, S.; Martinez-Pomares, L. The mannose receptor: linking homeostasis and immunity through sugar recognition. *Trends Immunol.* **2005**, *26*, 104−110.

DOI: 10.1021/acs.biomac.8b00305
Biomacromolecules XXXX, XXX, XXX−XXX

(27) van Vliet, S. J.; Saeland, E.; van Kooyk, Y. Sweet preferences of MGL: carbohydrate specificity and function. *Trends Immunol.* **2008**, *29*, 83−90.
(28) Geijtenbeek, T. B.; Gringhuis, S. I. Signalling through C-type lectin receptors: shaping immune responses. *Nat. Rev. Immunol.* **2009**, *9*, 465−479.
(29) Su, L.; Zhang, W.; Wu, X.; Zhang, Y.; Chen, X.; Liu, G.; Chen, G.; Jiang, M. Glycocalyx-Mimicking Nanoparticles for Stimulation and Polarization of Macrophages via Specific Interactions. *Small* **2015**, *11*, 4191−4200.
(30) Lundquist, J.; Toone, E. The Cluster Glycoside Effect. *Chem. Rev.* **2002**, *102*, 555−578.
(31) Austyn, J. M.; Gordon, S. F4/80, a monoclonal antibody directed specifically against the mouse macrophage. *Eur. J. Immunol.* **1981**, *11*, 805−815.
(32) Sica, A.; Mantovani, A. Macrophage plasticity and polarization: in vivo veritas. *J. Clin. Invest.* **2012**, *122*, 787−795.
(33) Mantovani, A.; Marchesi, F.; Malesci, A.; Laghi, L.; Allavena, P. Tumour-associated macrophages as treatment targets in oncology. *Nat. Rev. Clin. Oncol.* **2017**, *14*, 399−416.
(34) Sarhan, D.; Palma, M.; Mao, Y.; Adamson, L.; Kiessling, R.; Mellstedt, H.; Österborg, A.; Lundqvist, A. Dendritic cell regulation of NK-cell responses involves lymphotoxin-α, IL-12, and TGF-β. *Eur. J. Immunol.* **2015**, *45*, 1783−1793.
(35) Athie-Morales, V.; Smits, H.; Cantrell, A.; Hilkens, M. Sustained IL-12 Signaling Is Required for Th1 Development. *J. Immunol.* **2004**, *172*, 61−69.
(36) Ma, X.; Yan, W.; Zheng, H.; Du, Q.; Zhang, L.; Ban, Y.; Li, N.; Wei, F. Regulation of IL-10 and IL-12 production and function in macrophages and dendritic cells. *F1000Research* **2015**, *4*, 1465.
(37) Chang, C.-I.; Liao, J. C.; Kuo, L. Macrophage Arginase Promotes Tumor Cell Growth and Suppresses Nitric Oxide-mediated Tumor Cytotoxicity. *Cancer Res.* **2001**, *61*, 1100−1106.
(38) Gobert, M.; Treilleux, I.; Bendriss-Vermare, N.; Bachelot, T.; Goddard-Leon, S.; Arfi, V.; Biota, C.; Doffin, A. C.; Durand, I.; Olive, D.; Perez, S.; Pasqual, N.; Faure, C.; Ray-Coquard, I.; Puisieux, A.; Caux, C.; Blay, J.-Y.; Ménétrier-Caux, C. Regulatory T Cells Recruited through CCL22/CCR4 Are Selectively Activated in Lymphoid Infiltrates Surrounding Primary Breast Tumors and Lead to an Adverse Clinical Outcome. *Cancer Res.* **2009**, *69*, 2000−2009.
(39) Sakaguchi, S.; Yamaguchi, T.; Nomura, T.; Ono, M. Regulatory T cells and immune tolerance. *Cell* **2008**, *133*, 775−787.
(40) Sica, A.; Bronte, V. Altered macrophage differentiation and immune dysfunction in tumor development. *J. Clin. Invest.* **2007**, *117*, 1155−1166.
(41) Zhang, W.; Xu, W.; Xiong, S. Macrophage Differentiation and Polarization via Phosphatidylinositol 3-Kinase/Akt−ERK Signaling Pathway Conferred by Serum Amyloid P Component. *J. Immunol.* **2011**, *187*, 1764−1777.
(42) Vergadi, E.; Ieronymaki, E.; Lyroni, K.; Vaporidi, K.; Tsatsanis, C. Akt Signaling Pathway in Macrophage Activation and M1/M2 Polarization. *J. Immunol.* **2017**, *198*, 1006−1014.
(43) Jiménez-Garcia, L.; Herránz, S.; Luque, A.; Hortelano, S. Critical role of p38 MAPK in IL-4-induced alternative activation of peritoneal macrophages. *Eur. J. Immunol.* **2015**, *45*, 273−286.
(44) Gray, M. J.; Poljakovic, M.; Kepka-Lenhart, D.; Morris, S. M., Jr. Induction of arginase I transcription by IL-4 requires a composite DNA response element for STAT6 and C/EBPbeta. *Gene* **2005**, *353*, 98−106.
(45) O'Shea, J. J.; Pesu, M.; Borie, D. C.; Changelian, P. S. A new modality for immunosuppression: targeting the JAK/STAT pathway. *Nat. Rev. Drug Discovery* **2004**, *3*, 555−564.
(46) Takeda, K.; Tanaka, T.; Shi, W.; Matsumoto, M.; Minami, M.; Kashiwamura, S.; Nakanishi, K.; Yoshida, N.; Kishimoto, T.; Akira, S. Essential role of Stat6 in IL-4 signalling. *Nature* **1996**, *380*, 627−630.
(47) Lyons, A. B.; Parish, C. R. Determination of lymphocyte division by flow cytometry. *J. Immunol. Methods* **1994**, *171*, 131−137.
(48) Fazekas de St. Groth, B.; Smith, A. L.; Higgins, C. A. T cell activation: in vivo veritas. *Immunol. Cell Biol.* **2004**, *82*, 260−268.

DOI: 10.1021/acs.biomac.8b00305
Biomacromolecules XXXX, XXX, XXX−XXX